ELSEVIER

Journal of Alloys and Compounds 265 (1998) 49–55

Journal of ALLOYS AND COMPOUNDS

Thermomagnetic behaviors of Fe–Cr–N films with perpendicular magnetic anisotropy

Dong-Liang Peng, Kenji Sumiyama, Kenji Suzuki*

Institute for Materials Research, Tohoku University, Sendai 980, Japan

Received 18 June 1997

Abstract

The temperature dependence of magnetization has been determined for sputter-deposited Fe–Cr–N films with perpendicular magnetic anisotropy. Decomposition and phase transformation with heating have been determined by X-ray diffraction, differential scanning calorimetry, and thermomagnetometry. There are three magnetic transformation stages in the temperature-rising thermomagnetic curves. The first stage which occurs below 350°C corresponds to the paramagnetic transition of the ferromagnetic α-Fe–Cr phase. The second stage (350–550°C) is the decomposition of the α-Fe–Cr and nonmagnetic γ′-$(Fe,Cr)_4N_x$ phases into the pure α-Fe and σ-FeCr phases, leading to an increase of the magnetization and the disappearance of the perpendicular magnetic anisotropy. The final magnetic transformation stage is the paramagnetic transition (T_c=735°C) of the pure α-Fe phase. Since there is no rapid magnetization change between liquid helium temperature and room temperature, the γ′-$(Fe,Cr)_4N_x$ phase is nonmagnetic at low temperatures. © 1998 Elsevier Science S.A.

Keywords: Thermomagnetic behavior; Fe–Cr–N films; Perpendicular magnetic anisotropy

1. Introduction

Co–Cr films which exhibit a relatively large saturation magnetization and a high perpendicular magnetic coercivity have been extensively investigated since they are useful for perpendicular magnetic recording media with extremely high recording density [1–9]. However, the principal element is cobalt in this film which has a hcp structure. Recently, we have reported that Fe–Cr–N ternary films prepared by DC magnetron facing-target reactive sputtering have similar perpendicular magnetic anisotropy characteristics [10,11]. The films have a saturation magnetization of 300~400 emu cm^{-3} and a perpendicular coercivity of 800~1100 Oe. The microstructure and magnetic properties as well as the deposition parameter dependence have also investigated in detail by X-ray diffraction (XRD), scanning electron microscopy (SEM), transmission electron microscopy (TEM), magnetization, X-ray photoelectron spectroscopy (XPS) and Mössbauer effect [11,12]. The films consist of the ferromagnetic α-Fe–Cr (namely Fe-rich bcc structure) and nonmagnetic γ′-$(Fe,Cr)_4N_x$ ($x<1$) phases, and the enhancement of perpendicular anisotropy is always accompanied by a decrease in the grain size of α-Fe–Cr phase and growth of the γ′-$(Fe,Cr)_4N_x$ phase. In the Fe–Cr–N films with large perpendicular anisotropy, the γ′-$(Fe,Cr)_4N_x$ phase has columnar grains of about 20–40 nm in diameter and a strong (200) texture, while the α-Fe–Cr phase which has the pin-like shape grains with a size distribution of about 2–20 nm in diameter are located at the grain boundaries of the γ′-$(Fe,Cr)_4N_x$ phase. The origin of the perpendicular anisotropy is attributable to the shape anisotropy of the α-Fe–Cr fine grains.

In this paper, we reported thermomagnetic behaviors of the Fe–Cr–N ternary films prepared under different deposition condition. The change of the structure and magnetic properties after annealing at several temperatures have been investigated.

2. Experimental

Fe–Cr–N films were deposited on glass and aluminium foil substrates by facing-target-type DC magnetron sputtering in mixed $Ar+N_2$ plasma, using a composite target consisting of pure Fe (99.9%) and Cr (99.9%) plates. The alloy composition was adjusted by changing the Cr target area ratio, A_{Cr}, defined as A_{Cr}=[area of Cr]/[total area of Fe and Cr targets]. In order to obtain Fe–Cr–N films with

*Corresponding author.

0925-8388/98/$19.00
PII S0925-8388(97)00423-4

various nitrogen contents, a N_2 flow ratio, $R(N_2)$=[N_2-flow rate]/[Ar-flow rate+N_2-flow rate], was changed with mass flow controllers. The substrate temperature, T_s, during the sputtering deposition was kept at about 50°C by water cooling and at 150, 250 and 350°C by indirect resistive heating. The detailed sputtering conditions were described previously [10,11]. The chemical composition of deposited films was determined by inductively coupled plasma (ICP) optical emission spectrometry and helium carrier fusion–thermal conductivity methods. The annealing of as-prepared films is carried out in a vacuum of 5×10^{-5} Torr between 250 and 550°C for 15 min, where the heating and cooling rates are 10°C min^{-1}.

Structures of the films were analyzed by X-ray diffraction with CuKα radiation using a graphite monochromator. Magnetic properties of the films were measured by VSM with a maximum magnetic field of 16 kOe in the temperature range of 0~800°C, and by superconducting quantum interference device (SQUID) below room temperature. The measurement of all thermomagnetic curves above room temperature is carried out in a magnetic field of 10 kOe applied perpendicular to the film plane. The Curie temperature (T_c) and phase transformation temperature (T_f) are determined by extreme points of differential curves derived from thermomagnetic (M–T) curves. Thermal stability of the films were also determined by differential scanning calorimetry (DSC) in an argon gas flow at a heating rate of 10°C min^{-1}.

3. Results

3.1. Deposition parameter dependence of thermomagnetic curves

Fig. 1 shows the temperature dependence of magnetization (M–T curves) for the Fe–Cr–N films sputter-deposited at T_s=50°C, A_{Cr}=33% and different $R(N_2)$. The ICP measurement showed that the average concentration ratio of Fe and Cr in these films is insensitive to $R(N_2)$, being about 77:23. In Fig. 1a, the Curie temperature of the Fe–Cr film deposited at $R(N_2)$=0% (T_c) is 594°C, being lower than that (about 735°C) of a pure α-Fe film. Since X-ray diffraction results showed that this film is composed of the single α-Fe–Cr phase [12], the lower T_c can be ascribed to the antiferromagnetic interaction between Fe and Cr atoms at the nearest-neighbor position. In contrast to the Fe–Cr film, the temperature dependences of magnetization for the Fe–Cr–N ternary films deposited at $R(N_2)$=20, 30, 35 and 40% are much more complicated (as shown in Fig. 1b–e). Clearly, there are three magnetic transformation stages in temperature-rising curves of these films. In the first stage (below 350°C), the magnetic transition temperature, T_f, decreases with increasing $R(N_2)$: T_f=320, 290, 215 and 170°C for the films deposited at $R(N_2)$=20, 30, 35 and 40%, respectively. This

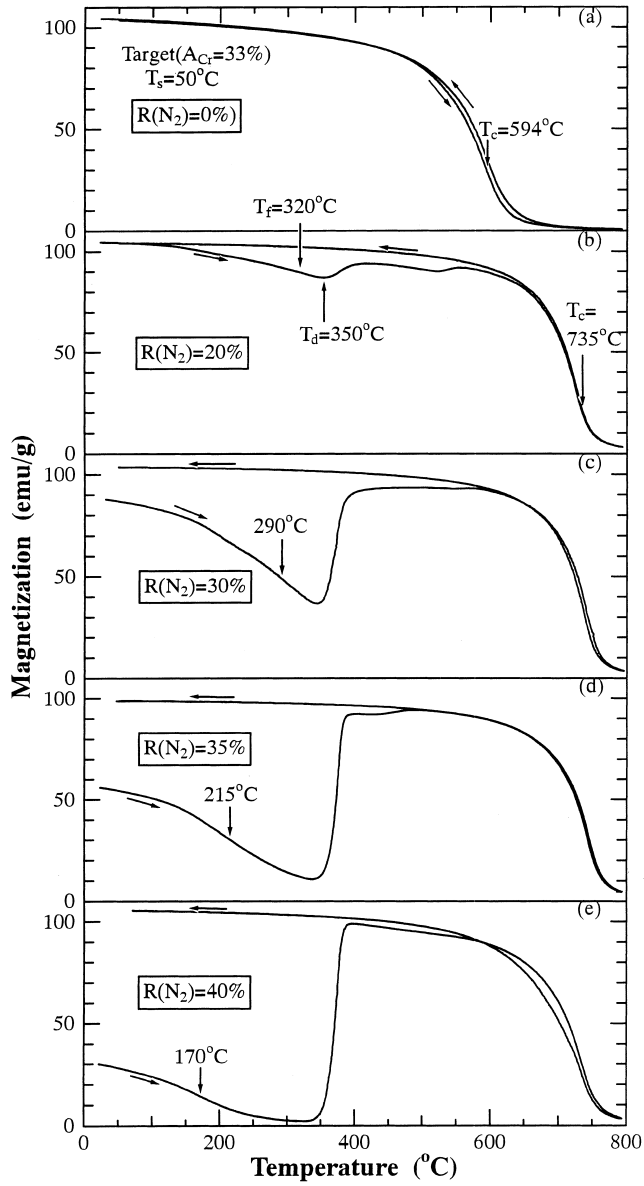

Fig. 1. Temperature dependence of the magnetization for Fe–Cr–N films sputter-deposited at T_s=50°C, A_{Cr}=33% and (a) $R(N_2)$=0, (b) 20, (c) 30, (d) 35 and (e) 40% in a magnetic field of 10 kOe.

magnetic transition is to the paramagnetic state of the ferromagnetic α-Fe–Cr phase because the γ′–$(Fe,Cr)_4N_x$ phase is nonmagnetic above room temperature [11]. The XRD results [12] indicate that the Fe–Cr–N films deposited at $R(N_2)$>0% consist of the nonequilibrium Fe-rich α-Fe–Cr and γ′-$(Fe,Cr)_4N_x$ phases, where the volume faction of two phases varies with $R(N_2)$. Therefore, the decrease of T_f with increasing $R(N_2)$ in the first stage is attributable to the increase of the Cr content in the α-Fe–Cr phase. The second magnetic transition behavior starts at about T_d=350°C and the magnetization steeply increases with increasing temperature. This stage is decomposition of the γ′-$(Fe,Cr)_4N_x$ and α-Fe–Cr phases, which is confirmed by the following X-ray diffraction results. The

final magnetic transition stage is to the paramagnetic state (T_c=735°C) of the pure α-Fe phase.

Fig. 2 displays that the M–T curves for films deposited at $R(N_2)$=35%, A_{Cr}=33% and different T_s. The M–T curves for the films deposited at T_s=150 and 250°C (Fig. 2b and Fig. 2c) are similar to that for the film deposited at T_s=50°C (Fig. 2a or Fig. 1d) and there are also three evident magnetic transition stages. But it is worth noting that the change in T_f is not obvious although the magnetization at room temperature decreases with increasing T_s. This suggests that the Cr content in the α-Fe–Cr phase is roughly the same for these deposited films and the nonmagnetic γ′-$(Fe,Cr)_4N_x$ phase is preferably formed at the higher T_s.

Fig. 3 shows the M–T curves for films deposited at

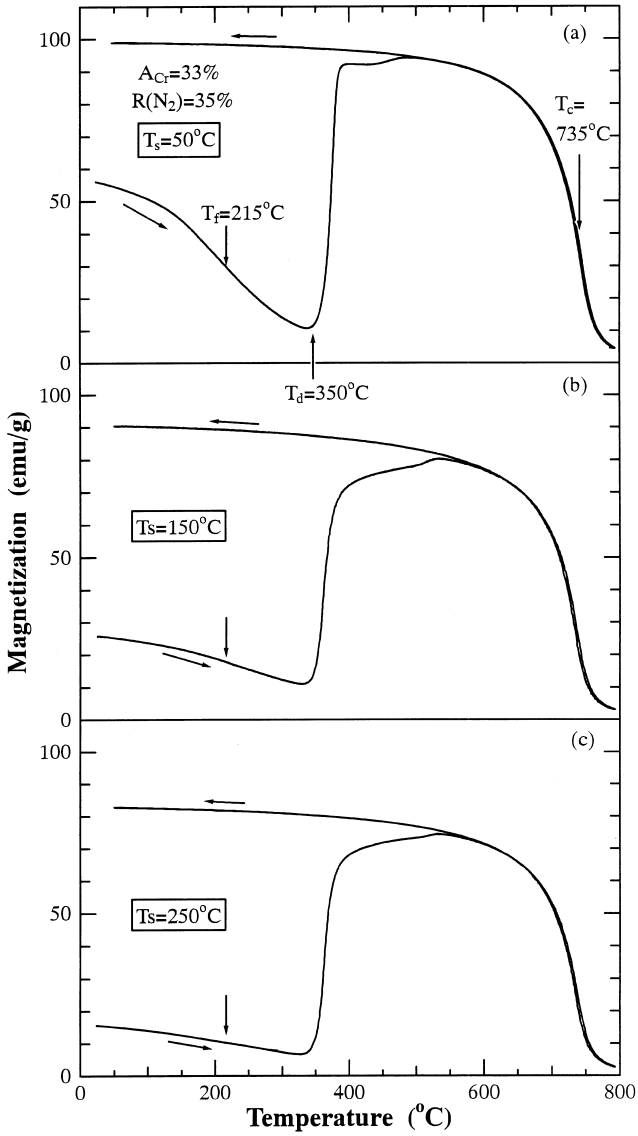

Fig. 2. Temperature dependence of the magnetization for Fe–Cr–N films sputter-deposited at $R(N_2)$=35%, A_{Cr}=33% and (a) T_s=50, (b) 150 and (c) 250°C in a magnetic field of 10 kOe.

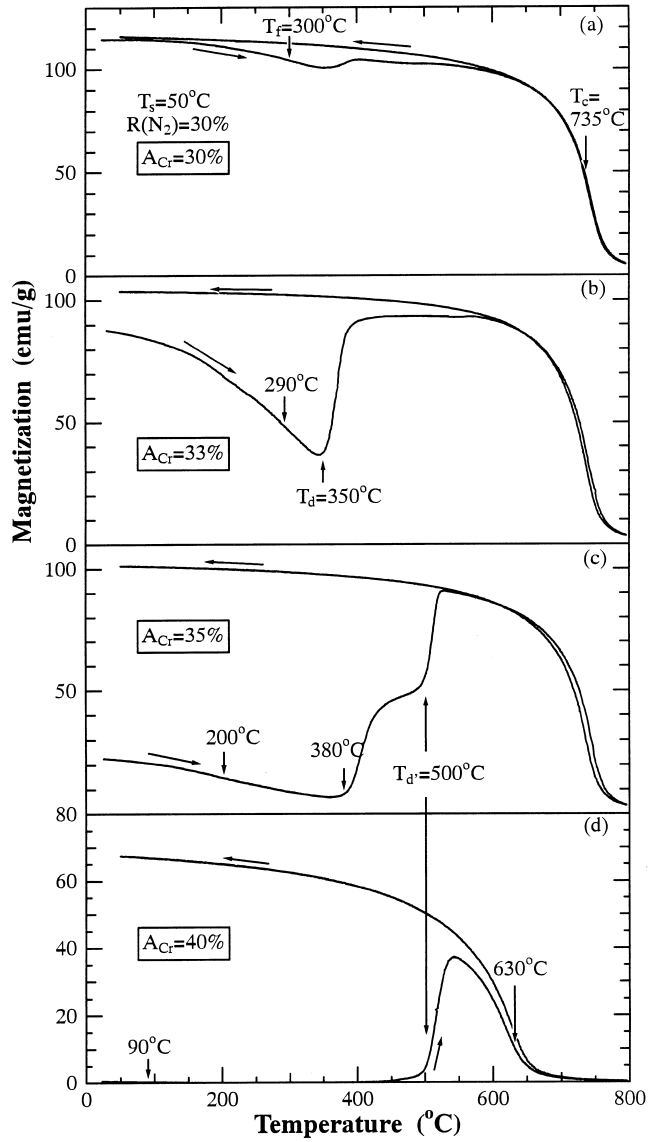

Fig. 3. Temperature dependence of the magnetization for Fe–Cr–N films sputter-deposited at $R(N_2)$=30%, T_s=50°C and (a) A_{Cr}=30, (b) 33, (c) 35 and (d) 40% in a magnetic field of 10 kOe.

T_s=50°C, $R(N_2)$=30% and different A_{Cr}. The ICP measurement shows that the nitrogen contents in these films are about 11 at.%. As can be seen here, the magnetization at room temperature decreases rapidly with increasing A_{Cr} and becomes almost zero at A_{Cr}=40%. The T_f also decreases rapidly with increasing A_{Cr}. This indicates that the Cr content in the α-Fe–Cr phase increases with increasing A_{Cr}. Note that, for the films deposited at A_{Cr}= 35% (Fig. 3c) and 40% (Fig. 3d), the temperature dependences of the magnetization are different from those of the films deposited at $A_{Cr}\leq$33%. There are two steep increase steps in Fig. 3c: the starting temperature of the first step is slightly higher than that in Fig. 3b, while that of the second step is the same as that in Fig. 3d: the decomposition temperature, $T_{d'}$, is about 500°C. In Fig. 3d, moreover, the

Curie temperature (T_c=630°C) of the final heating step is lower than that for $R(N_2)$≤35%.

In order to further determine what happens in these two stages, we measured XRD patterns of the films annealed at 300, 450 and 550°C for 15 min. Fig. 4a, Fig. 4b and Fig. 4c show XRD patterns of the films deposited at (a) A_{Cr}= 33%, (b) 35% and (c) 40%. Compared with the results for the as-deposited films, there are no evident changes in the XRD patterns for the films annealed at 300°C. For A_{Cr}= 33% (Fig. 4a), the γ′-$(Fe,Cr)_4N_x$ phase has completely decomposed into the pure α-Fe and Cr-rich α′-Cr–Fe (bcc) phases when annealed at 450°C. This result confirms that the magnetic transformation starting from T_d=350°C results from the decomposition of the α-Fe–Cr and γ′-$(Fe,Cr)_4N_x$ phases. After further annealing at 550°C, the α′-Cr–Fe phase slightly transforms into the pure α-Fe and σ-FeCr phases, causing a very small change in the magnetization as can be seen in Fig. 3b. For A_{Cr}=35% (Fig. 4b), annealing at 450°C leads to decomposition of the α-Fe–Cr phase and partial decomposition of the γ′-$(Fe,Cr)_4N_x$ phase into the pure α-Fe and α′-Cr–Fe phases. After annealing at 550°C, the retained γ′-$(Fe,Cr)_4N_x$ phase decomposes completely, and the α′-Cr–Fe phase also transforms completely into the pure α-Fe and σ-FeCr

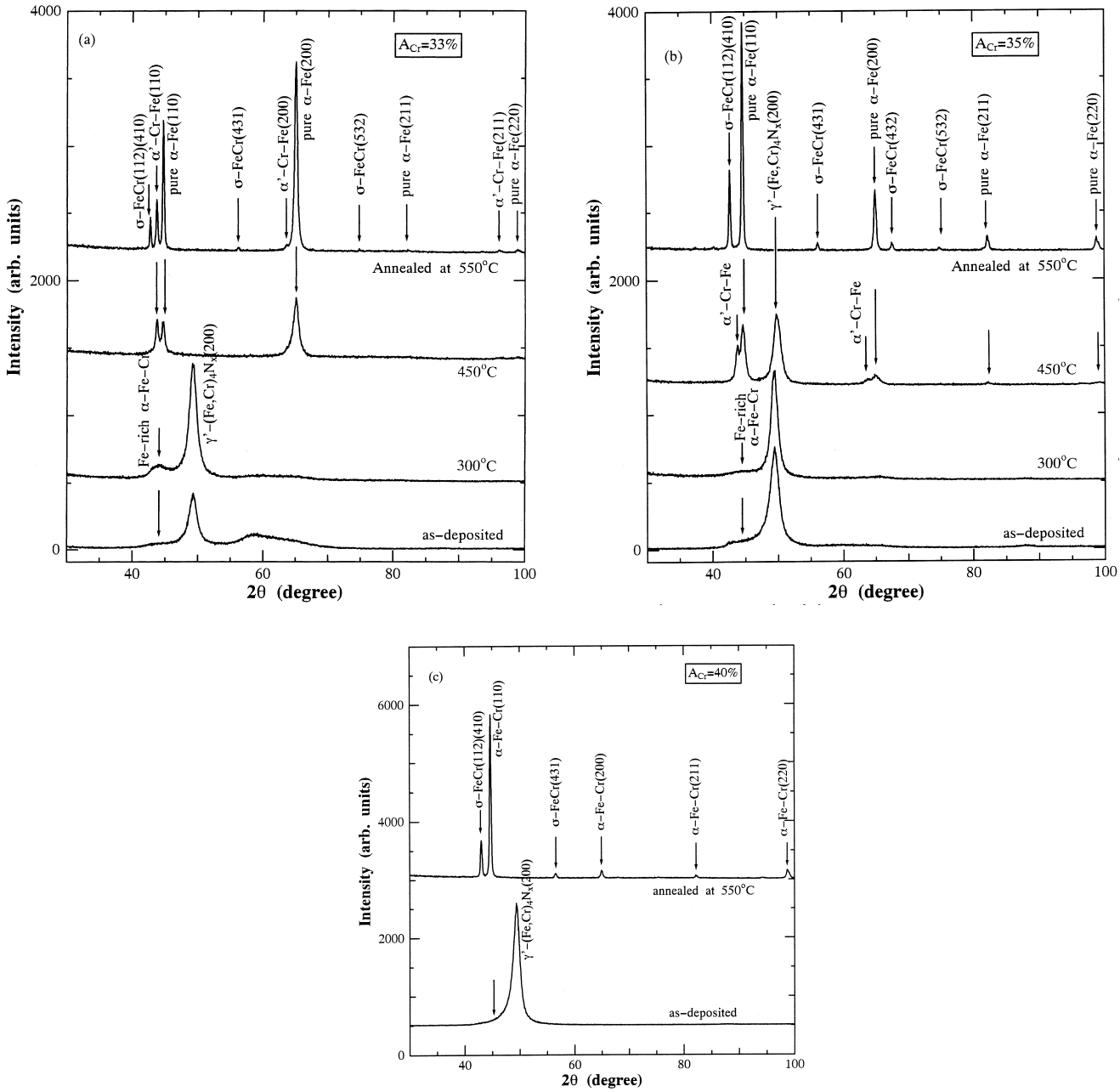

Fig. 4. X-Ray diffraction patterns of Fe–Cr–N films after annealing at 300, 450 and 550°C for 15 min. These films are deposited at $R(N_2)$=30%, T_s=50°C and (a) A_{Cr}=33, (b) 35 and (c) 40%.

phases, leading to a further increase in the magnetization. For A_{Cr}=40%, however, the decomposition of the γ′-$(Fe,Cr)_4N_x$ phase occurs at about $T_{d'}$=500°C because of the increase of the Cr content in the film. The XRD pattern after annealing at 550°C (Fig. 4c) indicates that the film consists of the σ-FeCr phase and the α-Fe–Cr phase but no pure α-Fe phase, leading to a lower Curie temperature, T_c=630°C, (see Fig. 3d).

3.2. Annealing temperature dependence of magnetization curves

Fig. 5 shows the magnetization curves of the $Fe_{71}Cr_{20}N_9$ film after annealing at (a) 250, (b) 300 and (c) 350°C for 30 min. This film was deposited at A_{Cr}=33%, $R(N_2)$=25% and T_s=250°C. As can be seen from Fig. 5a, the magnetization curve does not change after annealing at 250°C: the perpendicular coercivity, $H_{c\perp}$, is twice as large as the in-plane coercivity, $H_{c\parallel}$. The magnetization more easily saturates along the direction perpendicular to film plane than along the in-plane direction, displaying large perpendicular magnetic anisotropy. While the annealing temperature is above 250°C, the perpendicular anisotropy decreases and the saturation magnetization increases gradually with increasing annealing temperature. For the film annealed at 350°C (Fig. 5c), the in-plane direction becomes the preferred magnetization direction and the perpendicular anisotropy disappears. The XRD patterns of these annealed films are shown in Fig. 6. Before and after annealing at 250°C, the films have the same XRD patterns and are composed of the α-Fe–Cr and γ′-$(Fe,Cr)_4N_x$ phases. For the film annealed at 300°C, decomposition of a very small amount of the γ′-$(Fe,Cr)_4N_x$ phase results in a small change of the magnetization curves compared with the as-deposited film and the perpendicular anisotropy is still retained. But for the film annealed at 350°C, as can be seen from Fig. 6, the large amout of the nonmagnetic γ′-$(Fe,Cr)_4N_x$ phase has decomposed into the pure α-Fe and α′-Cr–Fe phases, which results in the disappearance of the perpendicular magnetic anisotropy.

3.3. Temperature dependence of magnetization below room temperature

Fig. 7 shows the temperature dependence of the magnetization for the $Fe_{71}Cr_{20}N_9$ film. It was measured in a SQUID magnetometer in an external magnetic field of 10 kOe from liquid helium temperature to room temperature. The fact that the magnetization decreases very slowly with increasing temperature and the absence of a steep change in the magnetization means that the paramagnetic transformation does not appear in the low temperature range, which indicates that the γ′-$(Fe,Cr)_4N_x$ phase is still nonmagnetic. Therefore, the perpendicular magnetic aniso-

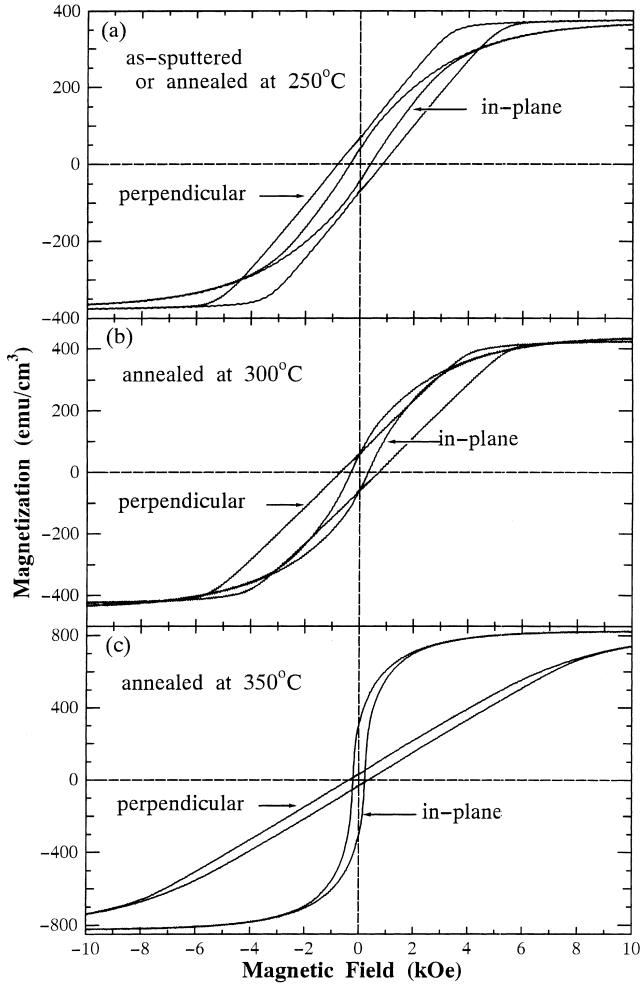

Fig. 5. Magnetization curves at room temperature for an $Fe_{71}Cr_{20}N_9$ film after annealing at (a) 250, (b) 300 and (c) 350°C for 30 min.

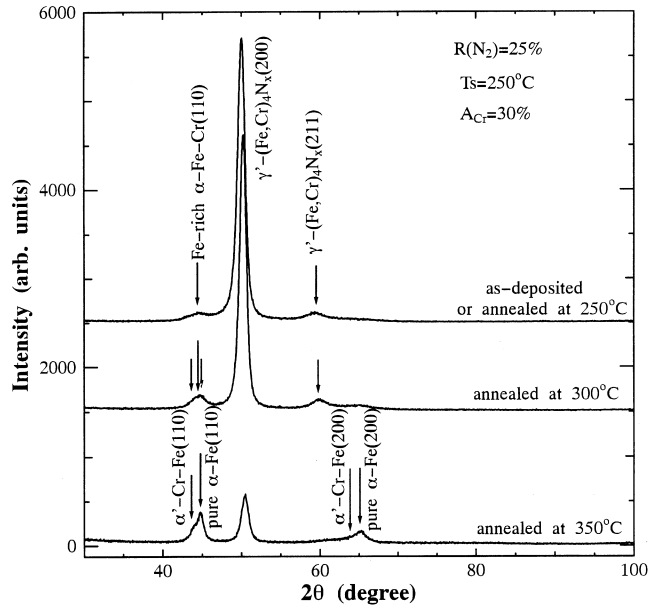

Fig. 6. X-Ray diffraction patterns of an $Fe_{71}Cr_{20}N_9$ film after annealing at (a) 250, (b) 300 and (c) 350°C for 30 min.

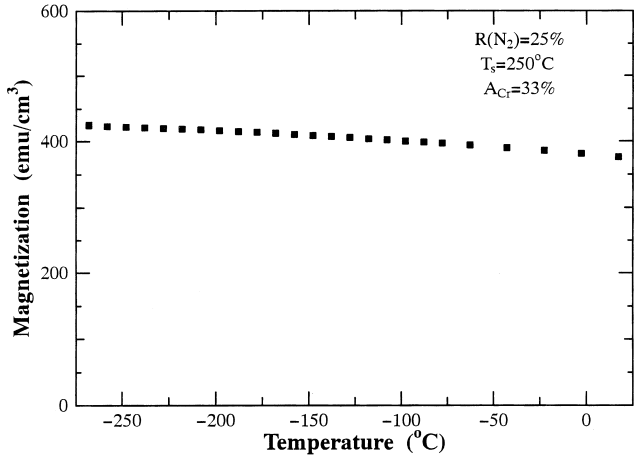

Fig. 7. Temperature dependence of the magnetization below room temperature for an $Fe_{71}Cr_{20}N_9$ film in a magnetic field of 10 kOe.

tropy of the film should be retained at low temperature. This is also confirmed further by the magnetization curves measured at liquid helium temperature (Fig. 8), showing the larger perpendicular coercivity ($H_{c\perp}$=1090 kOe) to be larger than that ($H_{c\perp}$=820 kOe) at the room temperature (Fig. 5a).

4. Discussion

As can be seen in Fig. 3, the increase of the Cr content evidently makes the decomposition temperature of the γ'-$(Fe,Cr)_4N_x$ phase higher: the γ'-$(Fe,Cr)_4N_x$ phase becomes more stable against heating. The XRD results show that under the same $R(N_2)$, the increase of A_{Cr} causes an increase in the amount of the γ'-$(Fe,Cr)_4N_x$ phase and the film deposited at A_{Cr}=40% which has an M_S value of about zero is almost entirely composed of the single γ'-$(Fe,Cr)_4N_x$ phase (see Fig. 4c). In order to obtain more

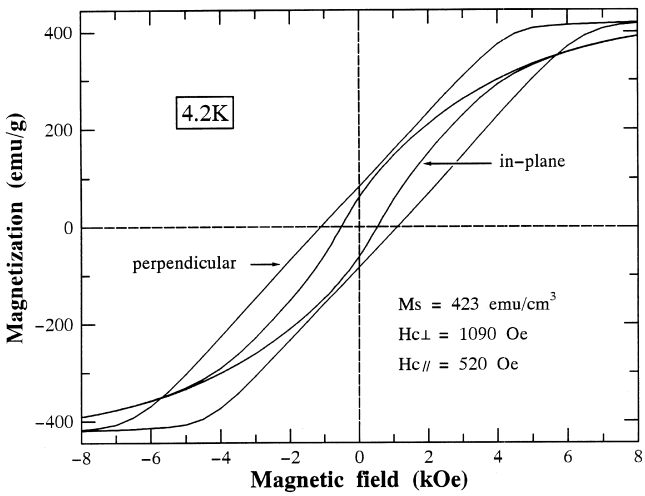

Fig. 8. Magnetization curves at liquid helium temperature for an $Fe_{71}Cr_{20}N_9$ film deposited at $R(N_2)$=25%, T_s=250°C and A_{Cr}=33%.

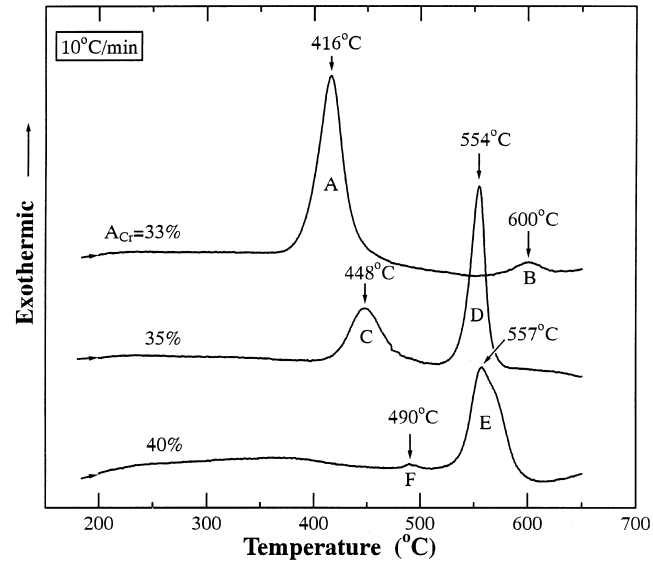

Fig. 9. DSC curves of the Fe–Cr–N films deposited at $R(N_2)$=30% and A_{Cr}=33, 35 and 40%.

information about the decompositions and phase transitions we have made an DSC analysis for the films deposited at A_{Cr}=33, 35 and 40% as shown in Fig. 9. For A_{Cr}=33%, the DSC curve shows a sharp exothermic peak (A) at 416°C (ΔQ_A=246.5 J g^{-1}) and a small broad exothermic peak (B) at 600°C (ΔQ_B=14 J g^{-1}). Clearly, the former corresponds to the decomposition of both α-Fe–Cr and γ'-$(Fe,Cr)_4N_x$ phases and the later to the formation of small amount of the σ-Fe–Cr phase (see Fig. 4a). For A_{Cr}=35%, there are also two peaks (C and D), corresponding to the two magnetization steps in the thermomagnetic curve (Fig. 3c). Because these two peaks are evidently independent or separated in Fig. 9, the broad peak at 448°C (ΔQ_C=85 J g^{-1}) is mainly attributed to the decomposition of the α-Fe–Cr phase and the sharp peak at 554°C (ΔQ_D=144 J g^{-1}) to the decomposition of the γ'-$(Fe,Cr)_4N_x$ phase. Similarly, for the film deposited at A_{Cr}=40%, there is a very small exothermic peak (F) at around 490°C (ΔQ_F=2.2 J g^{-1}), corresponding to the decomposition of very small amount of the α-Fe–Cr phase because the film is almost entirely composed of the single γ'-$(Fe,Cr)_4N_x$ phase. Furthermore, there is a large peak (E) at 557°C (ΔQ_E=164.5 J g^{-1}) which results from the decomposition of the γ'-$(Fe,Cr)_4N_x$ phase. Since the DSC curves of all samples in Fig. 9 show clear, large exothermic peaks, the nonequilibrium disordered α-Fe–Cr (bcc) and γ'-$(Fe,Cr)_4N_x$ (fcc) phases in the Fe–Cr–N films are decomposed via several transformation stages. The total DSC results are in good agreement with the results of the thermomagnetic measurements.

Since the cohesive energy between Cr and N ($|\Delta H_{CrN}|$= 62 kJ $mole^{-1}$) is larger than that between Fe and N ($|\Delta H_{Fe_4N}|$=16 kJ $mole^{-1}$) [13], we predict that the chromium nitride is more easily formed than the iron

nitride in the Fe–Cr–N films. However, under the present experimental conditions, though the Cr content is large (about 40at.%) and the maximum nitrogen content is about 18at.%, the γ'-$(Fe,Cr)_4N_x$ phase is formed instead of the CrN phase in the sputtered Fe–Cr–N films [12]. But the larger cohesive energy between Cr and N than between Fe and N may be one of the causes why the decomposition temperature of the nonequilibrium γ'-$(Fe,Cr)_4N_x$ phase increases with increase of the Cr content. The stability of the γ'-$(Fe,Cr)_4N_x$ phase also seems to be related to the decomposition of the surrounding α-Fe–Cr phase in the films. For the smaller A_{Cr}, the decomposition of a large amount of the α-Fe–Cr phase produce a large heat release. This induces the decomposition of the γ'-$(Fe,Cr)_4N_x$ phase (see Fig. 9: A_{Cr}=30%). For the larger A_{Cr}, because the size and amount of the α-Fe–Cr phase are smaller, such heat release is also small and not strong enough to induce the decomposition of the γ'-$(Fe,Cr)_4N_x$ phase (see Fig. 9: A_{Cr}=40%).

In addition, the size of the α-Fe–Cr grains decreases with increasing $R(N_2)$ and Cr content (A_{Cr}) [12]. Therefore, the size effect of the α-Fe–Cr grains, being of about nanometric size, may contribute to the decrease of T_f in Fig. 1 [14]. We have also observed superparamagnetic behaviors of the α-Fe–Cr phase for higher $R(N_2)$ and A_{Cr}. Detailed results will be discussed elsewhere.

In conclusion, the temperature dependence of magnetization for the Fe–Cr–N films with the perpendicular anisotropy demonstrates that the ferromagnetic α-Fe–Cr phase becomes paramagnetic above 350°C and that the decomposition of the γ'-$(Fe,Cr)_4N_x$ phase starts at about 350°C for $A_{Cr}\leq$35% and 500°C for A_{Cr}=40%. The magnetization curves and XRD patterns before and after annealing at 350°C indicate that the decomposition of the γ'-$(Fe,Cr)_4N_x$ phase causes the disappearance of the perpendicular magnetic anisotropy, implying a important role of the γ'-$(Fe,Cr)_4N_x$ phase on the perpendicular anisotropy in Fe–Cr–N films.

Acknowledgements

The authors thank to Dr. T. Takada and Mr. Y. Murakami for their help in the chemical analysis. One of the authors (D.L. Peng) appreciates the financial support from the Ministry of Education, Science, Culture and Sport, Japan. This work was also partially supported by Grant-in-Aid for General Scientific Research (No. 08405043) given by the Ministry of Education, Science, Culture and Sport, Japan.

References

[1] S. Iwasaki, Y. Nakamura, IEEE Trans. Magn. MAG 13 (1977) 1272.
[2] S. Iwasaki, K. Ouchi, IEEE Trans. Magn. MAG 14 (1978) 849.
[3] S. Iwasaki, K. Ouchi, T. Hizawa, J. Mag. Soc. Jpn. 9 (1985) 57.
[4] Y. Maeda, M. Asahi, J. Appl. Phys. 61 (1987) 1972.
[5] J.C. Lodder, L. Cheng-Zhang, J. Magn. Magn. Mater. 74 (1988) 74.
[6] K. Yoshida, H. Kakibayashi, H. Yasuoka, J. Appl. Phys. 68 (1990) 705.
[7] K. Takei, Y. Maeda, Jpn. J. Appl. Phys. 30 (1991) L1125.
[8] K. Hono, S.S. Babu, Y. Maeda, N. Hasegawa, T. Sakurai, Appl. Phys. Lett. 62 (1993) 2504.
[9] N. Honda, T. Chiba, K. Ouchi, IEEE Trans. Magn. MAG 31 (1995) 2758.
[10] D.L. Peng, K. Sumiyama, T.J. Konno, K. Suzuki, Jpn. J. Appl. Phys. 36 (1997) L479.
[11] D.L. Peng, T.J. Konno, K. Sumiyama, H. Onodera, K. Suzuki, J. Magn. Magn. Mater., in press.
[12] D.L. Peng, K. Sumiyama, M. Oku, T.J. Konno, K. Wagatsuma, K. Suzuki, submitted to J. Mater. Sci.
[13] F.R. de Boer, R. Boom, W.C.M. Mattens, A.R. Miedema, A.K. Niessen, Cohesion in Metals: Transition Metal Alloys, North-Holland, The Netherlands, 1988, pp. 177, 232.
[14] Y.W. Du, M.X. Xu, J. Wu, Y.B. Shi, H.X. Lu, J. Appl. Phys. 70 (1991) 5903.